THE ROLE OF MULLITE-BASED REFRACTORY CHEMICAL INTERACTIONS ON THE FORMATION OF EXOGENOUS NON-METALLIC INCLUSIONS

G. Cornacchia, M. Gelfi, C. Mapelli, A. Paderni, S. Panza, R. Roberti.

The occurrence of exogenous non metallic inclusions in steel is sporadic, but because of their large size, they have the most deleterious effect on steel properties, becoming the major cause of failure of mechanical components in service. These inclusions are usually entrapped in steel during teeming and solidification and tend to concentrate in the regions of the steel section that solidify most rapidly or in zones from which their escape by flotation is in some way hampered; in the case of forging ingots this region corresponds to the ingot bottom. The majority of exogenous inclusions originates from mould fluxes entrapment, reoxidation processes, which occur when molten steel comes into contact with external sources of oxygen, such as casting atmosphere, and refractories wear. Considering the large amount of inclusions sources, it is sometimes very difficult for a steelmaker to assess what is the precise origin of macroinclusions, in order to improve the process quality. This investigation is also complicated by the fact that the chemical characterization of macroinclusions is not easy, because the inclusions have large size and multiphase composition, with a chemical analysis which can change from point to point. For these reasons a careful analysis of this matter is always needed.
In the present work a precise characterization of macroinclusions which came from refractories, occurred in forging steel ingots, was carried out by means of SEM-EDS and non conventional X-Ray Microdiffraction technique. In order to explain the origin and the chemical evolution of these inclusions the analysis of ex-service refractory materials was carried out and a thermodynamical model taking in account the steel-refractory interactions was implemented.

KEYWORDS: *exogenous macro-inclusions, slag, refractory, calcium, ingot casting*

This study was carried out on 31-ton polygonal steel ingots. The fabrication process consists of the following steps: EAF tapping into refractory lined ladle, deoxidation of steel with aluminium in gas-stirring conditions, adjustment of the final composition, vacuum treatment, pouring of steel into an ingot mould by uphill casting. It takes about 80 min for the secondary metallurgy treatment, from tapping until casting.
The presence of macro-inclusions inside the polygonal ingots was discovered at the end of forging and rolling process, after ultrasonic investigations. The compositions of the two steel ingots (named ingot A and ingot B) affected by macro-inclusions considered in this study are reported in Tab. 1.
In order to investigate the influence of refractory wear on macro-inclusions formation, further heats of similar steel grade were considered. To analyse the refractory-steel interface, at the end of casting operations, different samples were sectioned from three positions of the ingot runner as shown in Fig. 1:

Giovanna Cornacchia, Marcello Gelfi, Roberto Roberti
Dipartimento di Ingegneria Meccanica, Università di Brescia, Via Branze, 38-25123 Brescia, Italy
Carlo Mapelli
Dipartimento di Meccanica, Politecnico di Milano, Via La Masa, 34-20156 Milano, Italy. E-mail: carlo.mapelli@polimi.it
Alberto Paderni, Silvano Panza
ASO SIDERURGICA s.r.l., Via Seriola,122-Ospitaletto, Italy

	%C	%Mn	%Si	%Cu	%Cr	%Ni	%Mo	%Al	%Ti
Cast I	0.30	0.51	0.33	0.14	1.09	0.24	0.22	0.023	.001
Cast II	0.18	0.67	.026	0.12	1.09	0.29	0.46	0.031	.002

Tab. 1

Compositions of the two steel ingots affected by macro-inclusions (wt%).

Composizione chimica dei due lingotti affetti da inclusioni riconducibili a materiale refrattario (wt).

	Al_2O_3	SiO_2	Fe_2O_3	MnO	CaO	MgO	K_2O	Na_2O	TiO_2
Refractory	67.2	26.8	1.58	0.01	0.37	0.29	0.47	0.13	2.19

Tab. 2

Refractory materials used for the vertical and the horizontal runners (wt).

Composizione chimica dei mattoni refrattari usati per la composizione dei canali della placca (wt).

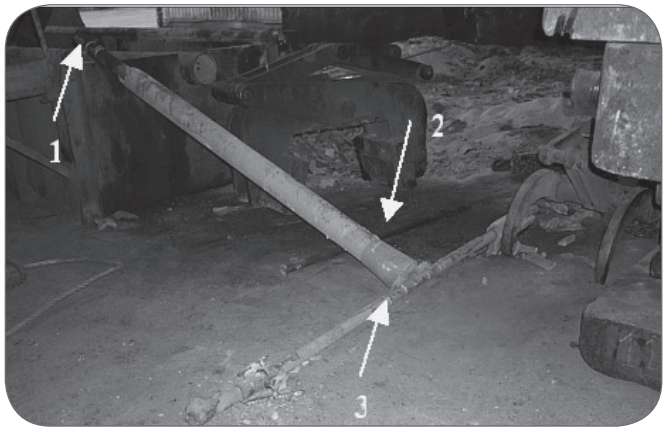

Fig. 1

Sampling positions of ingot runner.

Posizione di prelievo dei provini sui canali di colaggio.

– position 1, the upper part of vertical runner;
– position 2, the lower part of vertical runner;
– position 3, the beginning of horizontal runner, where the metal stream should be more turbulent.

The chemical compositions of refractory materials used for the ingot runners are shown in Tab. 2.

The chemical composition of the steel samples were examined using an Optical Emission (OE) spectrometer ARL3460.

The morphologies and chemical compositions of macroinclusions extracted from steel ingots were carried out by Scanning Electron Microscopy LEO mod. EVO 40XVP coupled to an Oxford EDS Microanalysis. In order to obtain the phase identification of inclusions, XRD data were collected by means of a D-Max Rapid Rigaku microdiffractometer with CuKα radiation. This apparatus is equipped with an Image Plate (IP) detector and it permits to focalise the beam on micro-areas, that is fundamental for studying small size samples as in this case. The irradiated area can be chosen by collimators of diameters from 800 to 10μ m. In this experiments a collimator diameter of 300μm was used. The acquisition time was fixed at 50 min, the voltage and current intensity were set at 30 kV and 40 mA respectively.

The mean composition of refractory materials was investigated by X-Ray Fluorescence ARL 9400. The steel samples cut from the runners were ground with silicon carbide paper and polished to mirror finishing, in order to examine the diffusion layers by means of SEM-EDS.

The in-situ observations of the evolution of the observed non metallic inclusions is not possible, so a thermodynamic model can be used to point out the possible origin of the observed non metallic inclusions on the basis of the chemical composition measured on the final solidified sample. The fundamental problem is to determine if the refractory can be a reliable source of the macro-inclusion featured by a high CaO and Al_2O_3, which usually causes the presence of not acceptable defects on the 35% of the discarded ingots which are refused because of the presence of the same defects. The refractories belong to the fundamental mullite ($3Al_2O_3 \cdot 2SiO_2$) system, so the significant presence of calcium revealed by the SEM-EDS analysis seems to exclude the involvement of the refractory materials, on the other hand the high frequency of this non metallic inclusions associated with the deterioration of the refractory of the pouring channel is well identified.

The thermodynamic interpretation is structured on the basis of the computation of the oxygen activity. The steels have not been treated by calcium, but the observed non metallic inclusions contain this element. This is certainly due to the high content and the related high activity of the lime within the slag used for the ladle furnace treatment (Tab. 3).

On the basis of the application of the data related to the activity of the lime within a complex slag analogous to the one used to treat the studied steels, the average activity lime can be stated around 0.02–0.036) and through the equilibrium relation this implies the presence of a Ca activity which can be defined by:

$$a_{Ca}=a_{CaO} / (K_{Ca\text{-}CaO}\, a_0) \qquad (1.1)$$

This computation of the calcium activity can be performed through Eq. (1.1) because the activity of the lime has been determined on the basis of the chemical composition of the slag, the activity of oxygen has been determined by the experimental measurements and the equilibrium constant (K_{Ca-CaO}) of the

	Al_2O_3	SiO_2	Fe_2O_3	MnO	CaO	MgO	Others
Slag	28.2	6.8	0.2	0.01	53.7	3.2	2.19

Tab. 3

Average chemical composition of the slag used during the refining period (wt).

Valori medi di composizione chimica della scoria impiegata durante l'affinazione dell'acciaio (wt)..

Chemical species	G^0 (J/mol)
Ca	-99.2T+44799
Al	-84.2T+42591
O	-145.2T-76028
CaO	-117.6T-580918
SiO_2	-134.5T-848440
Al_2O_3	-235.2T-1539859
$3CaO{\cdot}Al_2O_3$	-601T-3312118
$CaO{\cdot}2Al_2O_3$	-586T-3710542
$12CaO{\cdot}7Al_2O_3$	-3173T-17894624
$SiO_2{\cdot}CaO$	-256.4T-1463400
$SiO_2{\cdot}2CaO$	-364.2T-2069624
$2SiO_2{\cdot}CaO{\cdot}Al_2O_3$	-636T-3913789
$SiO_2{\cdot}2CaO{\cdot}Al_2O_3$	-612T-3700167
$3SiO_2{\cdot}3CaO{\cdot}Al_2O_3$	-911T-6187916
$SiO_2{\cdot}CaO{\cdot}Al_2O_3$	-479T-3063983

Tab. 4

Gibbs Standard energy for the chemical species involved in the considered chemical reactions (J/mol).
Valori di energia libera di Gibbs per le specie chimiche coinvolte nelle reazioni qui considerate (J/mol).

reaction which depends only on the temperature:

$$[Ca]+[O]\rightarrow(CaO) \quad (1.2)$$

The computation has been performed on the basis of the Gibbs Standard energies contained in Tab. 4 and on the basis of the activity coefficients shown in Tab. 5. The activities of the alloying elements have been computed on the basis of the chemical composition of the two studied steels recorded in Tab. 1. On the basis of the provided percentage weight concentration of the alloying elements, the molar fractions of these ones have been computed through their atomic masses.
The raoultian activity of the generic i species has been computed through:

$$a_i=\gamma_i X \quad (2.1)$$

where the activity coefficient is calculated according to:

$$\ln\gamma_i=\ln\gamma_i^0+\sum_j \epsilon_i^j[Xj] \quad (2.2)$$

where the applied activity coefficients at infinite dilution and the interaction ones are collected in Tab. 5 according to the literature data.
Provided an average raoultian activity of oxygen measured by an electrochemical concentration cell (Celox) at the end of the ladle treatment of $5.7 \cdot 10^{-6}$ and an average pouring temperature of 1 570–1 580°C, the steel is always interested by a raoultian Ca activity of $4.6 \cdot 10^{-5}$ which corresponds to a Ca mass concentration of 9 ppm (Appendix A), because the raoultian activity coefficient of calcium in the treated situation has been estimated to be $\gamma Ca=3.7$.
The high calcium activity interesting the steel bath can be provided also by the fragments of the refining slag trapped on the ladle refractory linings. These fragments are featured by a chemical compositions nearly equal to the one of the refining slag and are in contact also with the deepest layers of the steel

The activity coefficients and the interaction parameters	Expression as a function of temperature	Reference
$\ln\gamma_{Al}^0$	0.0025*T*-13.51	10)
$\ln\gamma_{Ca}^0$	0.0085*T*-8.95	11)
$\ln\gamma_O^0$	0.0046*T*-14.34	12)
ε_O^{Al}	8.1	10)
ε_O^{Fe}	63399/T-27	12)
ε_O^{C}	-20	13)
ε_O^{Cr}	499000/T-281	12)
ε_O^{Co}	-6	11)
ε_O^{Mn}	-5.7	12)
ε_O^{O}	-115000/T+50	12)
ε_O^{S}	-35.5	13)
ε_O^{Si}	-37099/T+8.9	12)
ε_{Al}^{Al}	4.67	13)
ε_{Al}^{C}	34.7	13)
ε_{Al}^{Ca}	8	14)
ε_{Al}^{Mn}	14.1	13)
ε_{Al}^{Si}	22.2	13)
ε_{Al}^{S}	11.6	13)
ε_{Ca}^{S}	-32660	14)
ε_{Ca}^{Si}	39.4	14)

Tab. 5

Activity coefficients based on mole fraction applied to Al, Ca and O to take into account their non-ideal behaviour in solution in iron.
Coefficienti di attività basati sulla frazione molare applicati ad Al, Ca e O per valutare un comportamento non ideale all'interno della soluzione di acciaio.

within the ladle and such a situation favours a high activity of calcium also in this regions which are very far from the slag interface. The deposition of the slag layer on the refractory linings has been proved by the experimental evidences that point out the presence of the slag traces (about 1–2 mm thick) deposited during the empting of the former heats treated within the same ladle.
So, within the steel there is a presence of calcium which surely can interact with the non metallic materials of the inclusions and of the refractories. The hypothesis which needs to be verified from a thermodynamic point of view is the transformation which leads from the refractory composition to the ones featuring the non metallic inclusions, in which Ca can play a fundamental role.
The computational thermodynamic model structured to evaluate this item is based on the thermodynamic driving force which is available for the different possible chemical reactions and it has already applied to the forecasting of the non metallic inclusions belonging to the ternary system CaO–SiO2–Al_2O_3.[7]
The thermodynamic driving force of the considered reactions is determined through the evaluation of the oxygen activity characterizing the equilibrium of each reaction. The sequence of the reactions can proceed only from a reaction featured by a higher oxygen activity to the one featured by a lower oxygen activity, because the needed driving force for the development is available only in this case. The set of the considered reaction:

$$(3Al_2O_3{\cdot}2SiO_2)+4[Ca]+4[O]\rightarrow(SiO2{\cdot}2CaO{\cdot}Al_2O_3)+(Al_2O_3) \quad (3.1)$$

$(3Al_2O{\cdot}2SiO2)+3[Ca]+3[O]\rightarrow(CaO{\cdot}2Al_2O_3)+(2CaO{\cdot}SiO2)+(Al_2O_3)+(SiO_2)$ (3.2)

$2(SiO_2)+(Al_2O_3)+[Ca]+4[O]\rightarrow(2SiO_2{\cdot}CaO{\cdot}Al_2O_3)$ (3.3)

$(SiO_2)+(Al_2O_3)+2[Ca]+2[O]\rightarrow(SiO2{\cdot}2CaO{\cdot}Al_2O_3)$ (3.4)

$3(SiO_2)+(Al_2O_3)+3[Ca]+3[O]\rightarrow(3SiO_2{\cdot}3CaO{\cdot}Al_2O_3)$ (3.5)

$2(Al_2O_3)+[Ca]+[O]\rightarrow(CaO{\cdot}2Al_2O_3)$ (3.6)

$7(Al_2O_3)+12[Ca]+12[O]\rightarrow(12CaO{\cdot}7Al_2O_3)$ (3.7)

$(Al_2O_3)+3[Ca]+3[O]\rightarrow(3CaO{\cdot}Al_2O_3)$ (3.8)

$(SiO_2)+[Ca]+[O]\rightarrow(CaO{\cdot}SiO_2)$ (3.9)

and the constant of equilibrium of each reaction has been computed on the basis of the standard free energy (G0) of each involved chemical species (Tab. 4).[8,9] The activity coefficients have been applied to the mole fraction of the alloying elements considered in the reactions to take into account their non ideal behaviour in the iron solution (Tab. 5).[10–14]
The activity of the chemical species on the right side of the reaction has been considered with an activity of 1, because they have found it in a nearly pure state during the experimental examinations. The relations (3.1) and (3.2) describe the possible aggression process of the Ca against the mullite refractories which implies also the formation of pure Al_2O_3 and SiO_2 which have been individuated in great quantity. In all the chemical reactions there is the presence of calcium within the left side reactant species, because the presence of this alloying element is implied by Eq. (1.1) and confirmed by the observation performed within the non metallic inclusions, while the reactant SiO_2 and Al_2O_3 represent the species formed by the reactions (3.1) and (3.2) and so their activities have been considered with value of 1. This last assumption has been set to maintain a consistence with the hypothesis operated for the computation of reactions (3.1) and (3.2) in which SiO_2 and Al_2O_3 on the right side of the reaction have been considered as pure on the basis of the experimental observations which confirmed the presence of pure SiO_2 and Al_2O_3 probably formed by the damage of the refractories. The development of the reaction sequence should follow the oxygen potential from the highest one to the lowest one.
Fig. 2 and 3 show the optical and electron microscopy images of the macro-inclusions extracted from the steel ingots A and

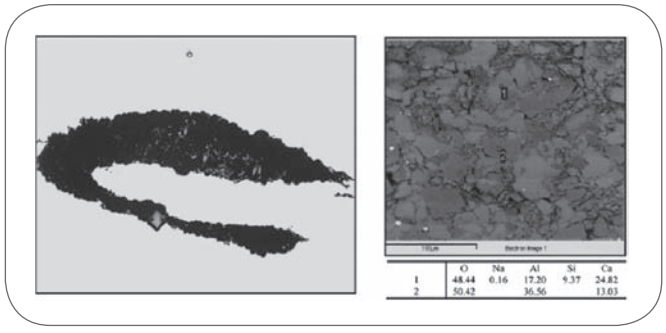

Fig. 2

Macro-inclusion A. On the right: optical image (magnification 30_), on the left: SEM image in back-scattering mode and EDS analyses (wt%).
Macro inclusione dal lingotto A: sulla destra l'immagine ottica (30X) e sulla sinistra l'immagine SEM (modalità back-scattering) con analisi EDS (wt).

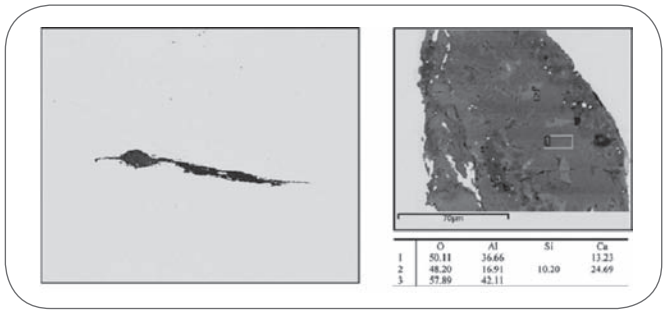

Fig. 3

Macro-inclusion B. On the right: optical image (magnification 30_), on the left: SEM image in back-scattering mode and EDS analyses (wt%).'
Macro inclusione dal lingotto B: sulla destra l'immagine ottica (30X) e sulla sinistra l'immagine SEM (modalità back-scattering) con analisi EDS (wt).

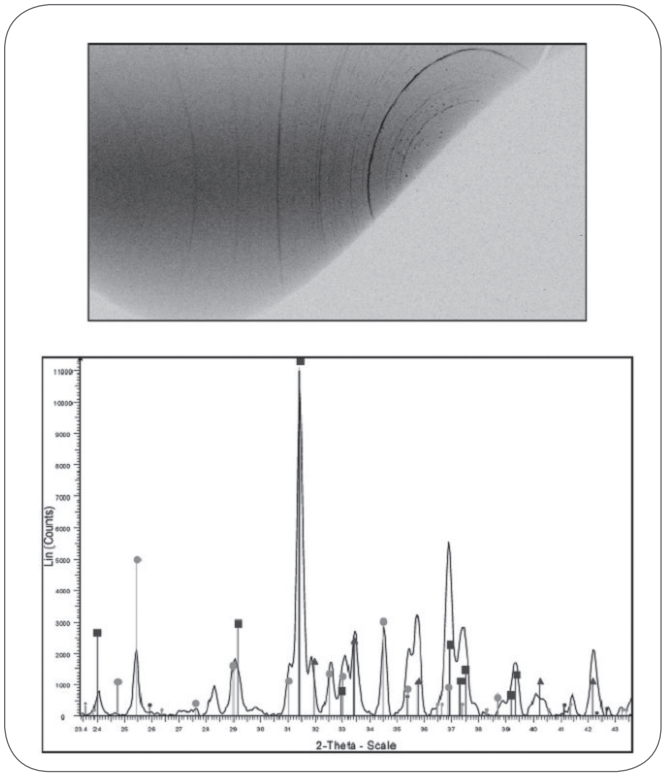

Fig. 4

2D diffraction image and integrated pattern collected from macro-inclusion A. The squares represent the gehlenite Ca2Al(AlSiO7) (JC-PDF card. N° 771113) phase contribution, the circles and the triangles represent the grossite $CaAl4O7/CaO{\cdot}2Al_2O_3$ (JC-PDF card. N° 231037) and the alumina Al_2O_3 (JC-PDF card. N° 100414) phases contribution respectively.
Immagine 2D della diffrazione ai raggi X e modello integrato ricavato dalla macroinclusione A: il quadrato rappresenta la fase di gelenite Ca2Al(AlSiO7), cerchi e triangoli rappresentano grossite $CaAl4O7/CaO{\cdot}2Al_2O_3$ e allumina Al_2O_3 rispettivamente.

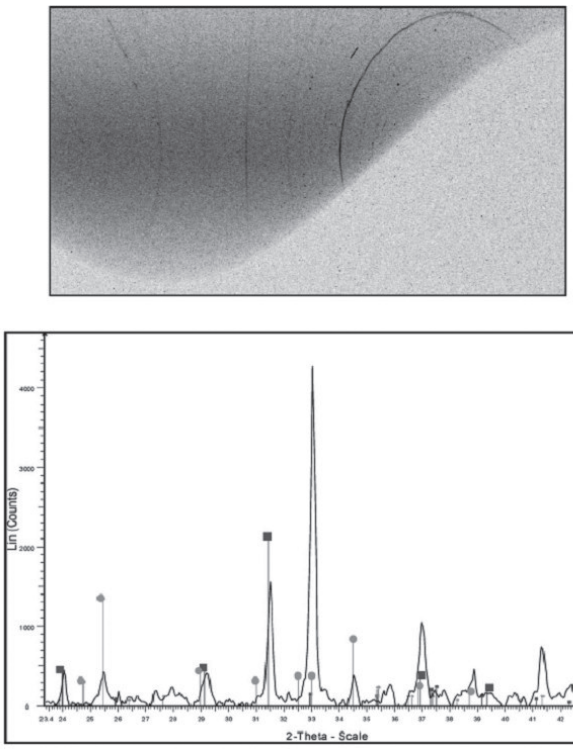

Fig. 5

2D diffraction image and integrated pattern collected from macro-inclusion B. The squares and the circles represent the gehlenite Ca2Al(AlSiO7) (JC-PDF card. N° 771113) and the grossite CaAl4O7/CaO· 2Al$_2$O$_3$ (JC-PDF card. N° 231037) phases contribution respectively.

Immagine 2D della diffrazione ai raggi X e modello integrato ricavato dalla macroinclusione B: il quadrato rappresenta la fase di gelenite Ca2Al(AlSiO7), cerchi e triangoli rappresentano grossite CaAl4O7/CaO·2Al$_2$O$_3$ e allumina Al$_2$O$_3$ rispettivamente.

B respectively. These inclusions appear to be multiphase, they have similar chemical composition, which consists mainly of calcium– aluminium silicates and calcium aluminates. In the case of inclusion from steel B, the EDS micro-analysis evidenced also the presence of a phase containing only Al and O, probably alumina (Al_2O_3).

The results of bidimensional X-ray diffraction confirmed the presence of these phases inside the inclusions and revealed their crystalline nature. In Fig. 4 the 2D diffraction image and the integrated pattern collected from macro-inclusion A is reported. It is possible to distinguish the phase contribution of gehlenite $Ca_2Al(AlSiO_7)$ (JC-PDF card. n° 771113), grossite $CaO{\cdot}2Al_2O_3$ (JC-PDF card. n° 231037) and alumina Al_2O_3 (JC-PDF card. n° 100414).

The relative intensities of diffraction peaks related to these crystalline phases differ from the tabulated ones, because there are only a few diffracting domains and as a consequence of fluorescence coming from the steel matrix. Despite the low intensity of diffraction peaks, also in the case of macro-inclusion B, the integrated diffraction pattern permits to assess the presence of gehlenite and grossite phases, as reported in Fig. 5.

Considering that the steel is deoxidised by aluminium without calcium addition and that the ladle is lined with Mg–O bricks,

%weight concentration							
STEEL A				STEEL B			
Al_2O_3	CaO	SiO_2	Other species with presence of Fe, Cr, Mn.	Al_2O_3	CaO	SiO_2	Other species with presence of Fe, Cr, Mn.
92.2	4.4	2.2	1.9	88.4	5.2	2.2	1.9
92.8	4.5	2.3	0.4	94.3	4.3	1	0.4
90.1	4.3	3.1	2.5	91.5	4.6	3.1	0.8
91.8	4.4	1.7	2.1	93.8	6	0	0.2
93.4	4.5	1.8	0.3	92.2	4.2	1.8	1.8
91.2	4.6	2.6	1.6	90.6	4.1	2.6	2.7
88.8	4.8	2.8	3.6	91.6	4.6	2.8	1
90.8	4.7	1.8	2.7	89.6	4.8	1.8	3.8
93.3	4.3	0.6	1.8	87.2	7.2	2.5	3.1
100	0	0	0	91.6	5	0	3.4
90.2	5.8	3.1	0.9	92.7	4.8	2.1	0.4
86.3	6.9	4.6	2.2	98.2	1	0	0.8
89.1	4.5	2.1	4.3	88.1	4.5	2.1	5.3
91.3	4.6	2.2	1.9	87.8	3.7	2.2	6.3
90	4.3	1.4	4.3	90.8	4.4	1.4	3.4

Tab. 6

Chemical composition of the inclusions featured by an average diameter smaller than 3m m found in steel A and in steel B.

Composizione chimica delle inclusioni caratterizzate da un diametro medio inferiore a 3mm trovate nell'acciaio A e nell'acciaio B.

one can expect that the endogenous inclusions should be principally Al_2O_3 and spinel ($MgO{\cdot}Al_2O_3$),15) but in the studied case the CaO-based slag used for the treating of the steels changes significantly the conditions which are more similar to the ones tested by Todoroki et al.16) who pointed out also endogenous inclusions containing CaO in steel deoxidised only by Al. The experimental observations performed on 30 examples of the non metallic inclusions featured by an equivalent diameter under 3μm have confirmed the presence of calcium, actually they show an average weight concentration of alumina in the range of 91.3% (st. dev. 2.9%) and an average one of CaO of 4.5% (st. dev 1.4%) (Tab. 6); the inclusions of little size have been considered as more characteristic of the endogenous population and their composition is certainly more similar to the one of the compounds nucleated by the liquid phase, because they certainly undergo a more contained growth process interested by the interaction among the firstly precipitated compounds and the transforming elements. However, it is worth noting that the presence of calcium also in these inclusions is probably the effect of the calcium activity imposed by the equilibrium between the liquid steel and the slag computed through Eq. (1.1), because this level of calcium activity can perform a transformation also of the endogenous compounds, in which the Al_2O_3 combines with CaO to produce other complex phases. So, we can conclude that the analysed macro-inclusions containing high percentages of calcium and silicon are of exogenous origin. In order to evaluate if the interaction between the liquid steel and the refractory materials of ingot runners can produce this type of macro-inclusions, some steel-refractory samples were sectioned as above mentioned.

The longitudinal section of ingot runner presents four layers with different morphology and chemical composition (Fig. 6). Moving from the inner towards the outside, these layers are:

- steel (area A), with the same composition of the steel ingot;
- steel-refractory interface (area B), characterized by the entrapment of refractory materials in form of single particles or as thin branched networks;
- modified refractory layer (area C), rather adherent to the steel; it presents a chemical composition quite different from the original one;
- refractory layer (area D), which maintains the original properties and chemical composition.

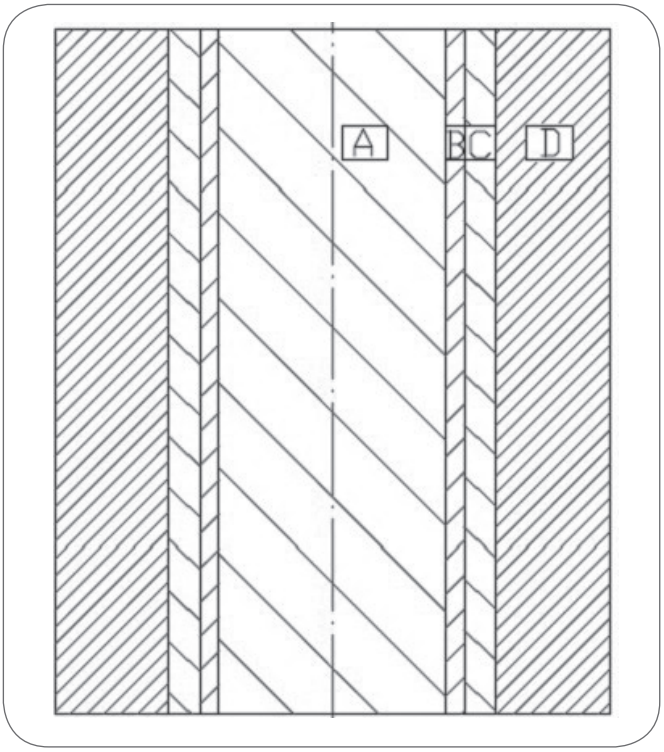

Fig. 6

Sketch of the longitudinal section of ingot runner.
Schema della sezione longitudinale dei canali della placca dopo il colaggio.

These four layers are not always clearly distinguishable, especially in the case of the two samples taken from the vertical runner, where the area C is very thin and adherent to steel, probably because of small interactions between refractory and liquid steel.
The refractory layers were separated from the steel, when it was possible, and analysed by X-ray fluorescence. The results are reported in Tab. 7. As expected, the first layer D has a composition close to the original one for both horizontal and vertical runner. On the contrary, the area C taken from the horizontal runner has lower content of SiO2 and higher content of Fe_2O_3, Al_2O_3 and MnO in respect to the original composition. This is a consequence of exchange reactions which take place, in the solid phase at temperature close to 1 600°C, between Al_2O_3–SiO_2 base refractory and aluminium-killed molten steel as also reported by the other authors.17) Fe, Mn and a small amount of Al contained into liquid steel, in contact with the refractory, can replace Si in the silica, producing this compositional change.

	VERTICAL RUNNER		HORIZONTAL RUNNER		
	As-produced	Area D (*)	As-produced	Area D	Area C
Al_2O_3	67.2	66.98	70.7	70.57	73.01
SiO_2	26.8	27.02	23.8	23.85	16.79
Fe_2O_3	1.58	1.46	1.55	1.45	5.03
MnO	0.01	0.03	0.01	0.02	0.23
CaO	0.37	0.29	0.31	0.27	0.28
MgO	0.29	0.29	0.30	0.29	0.24
K_2O	0.47	0.49	0.51	0.53	0.46
Na_2O	0.13	0.18	0.22	0.27	0.28
TiO_2	2.19	2.24	1.89	1.88	1.72

Tab. 7

Compositional comparison between runners refractory before and after casting (wt%) (*) The chemical composition is the mean between sample taken from position 1 and 2.
Comparazione della composizione chimica dei refrattari dei canali prima e dopo il colaggio (wt) [*] La composizione chimica è il risultato della media tra i campioni presi dalle posizioni 1 e 2.

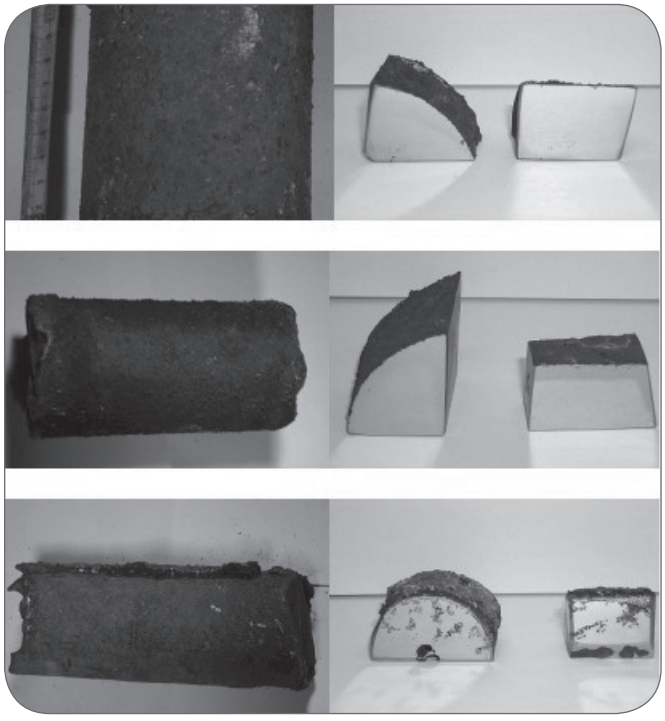

Fig. 7

Steel samples taken from ingot runners in positions 1, 2 and 3, after refractory removal (on the left) and after sectioning and olishing (on the right).
Campioni di acciaio prelevati dai canali di colaggio nelle posizioni 1,2 e3 dopo la rimozione del materiale refrattario (a sinistra) e dopo il sezionamento e la pulimentazione (a destra).

In order to analyse the interaction area B, the metallic samples, free from refractory, were sectioned and polished to mirror finishing. Fig. 7 shows the pictures of the these three samples. The visual inspection shows that the steel taken from the vertical runner (samples 1 and 2) had only a small interaction with the refractory, which is limited to the outer contour of the steel section as a thin crust with a uniform thickness.
On the contrary, in the sample 3, taken from the horizontal runner, the interaction layer is very large, confirming the hypothesis that in this area, where the steel flow is turbulent, the refractory is more affected by chemical and mechanical erosion. As a consequence, there is the evidence of large non-metallic particles inside the steel, which are completely detached from the refractory lining and appear to be free to enter the mould producing macro-defects.
For this reason the SEM-EDS analysis was concentrated on sample 3, scanning the composition of the steel-refractory interaction area step by step from outside to the centre of the channel section (Figs. 8(a)–8(d)).
The starting point of this analysis (Fig. 8(a)) shows that the

a

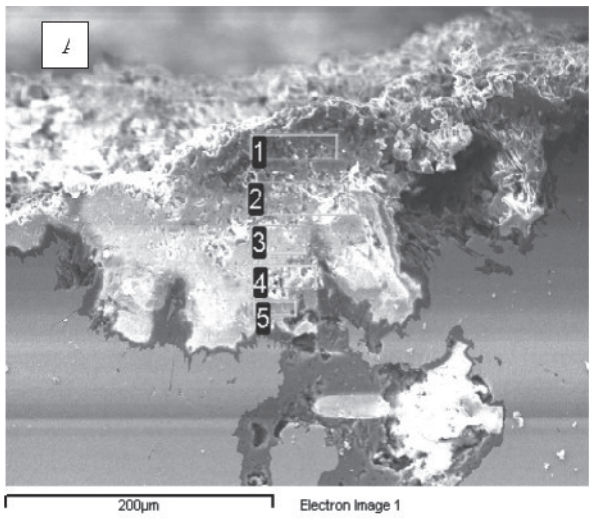

Spectrum	O	Na	Mg	Al	Si	Ca	Ti	Mn	Fe
1	51.45		4.89	36.13	0.73	0.51	0.89	2.22	3.19
2	50.75	0.60	3.26	36.06	0.75	1.30	0.95	2.01	4.33
3	54.92		1.00	33.39	1.88	4.08	1.41	0.32	3.01
4	53.44	0.41	0.66	33.06	2.30	4.84	1.09		4.20
5	53.59		0.61	36.10	2.29	5.33	0.50	0.34	1.25

c

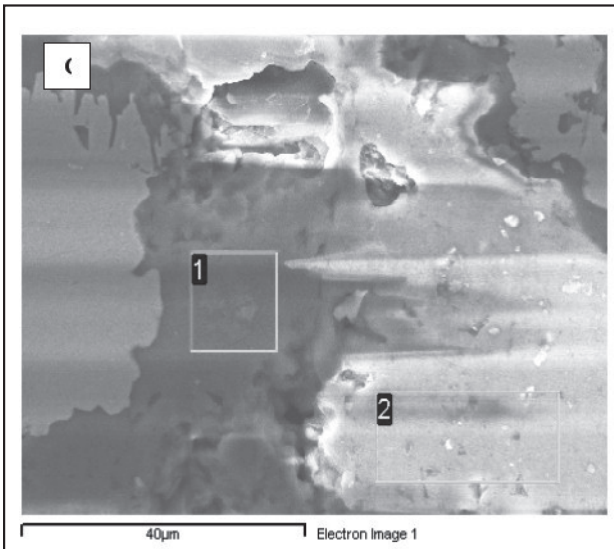

Spectrum	O	Na	Mg	Al	Si	Ca	Mn	Fe
1	49.68	1.15	0.66	36.56	0.46	11.50		
2	52.03		2.97	34.42	0.43	9.09	0.55	0.49

b

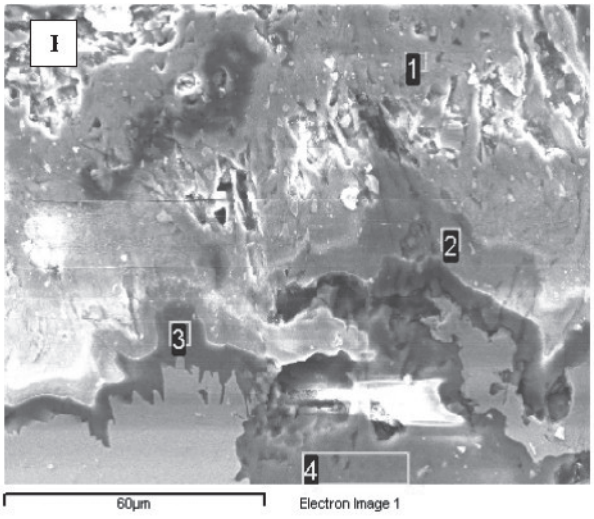

Spectrum	O	Mg	Al	Si	Ca	Ti	Mn	Fe
1	59.68	1.05	34.19	1.03	2.81	0.98	0.26	
2	55.42	0.54	36.40	1.92	5.11	0.61		
3	52.95	0.53	34.35	3.43	6.32	0.66	0.85	0.90
4	54.87	1.70	33.75	0.57	8.75		0.36	

d

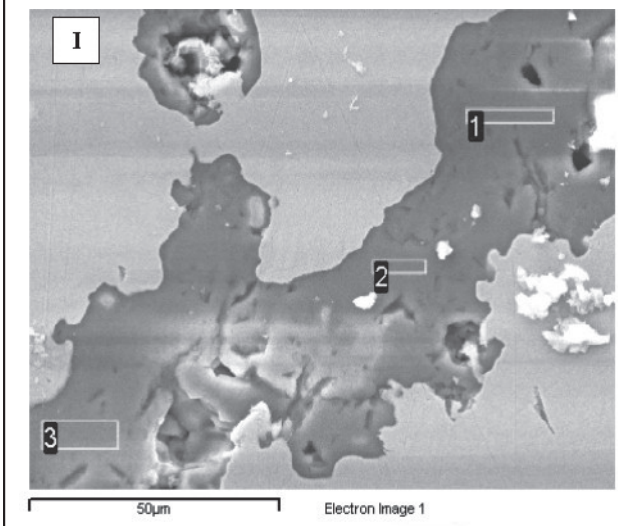

Spectrum	O	Al	Ca
1	51.55	36.72	11.73
2	50.24	37.09	12.67
3	49.91	37.30	12.79

▲ *Fig. 8*

Secondary SEM images and EDS analyses (wt%) of steel-refractory interaction layer in the sample sectioned from the horizontal runner (position 3).

Immagini SEM e analisi EDS (wt) dello strato di interazione tra acciaio e refrattario sulla sezione del campione prelevato dal canale orizzontale (pos.3).

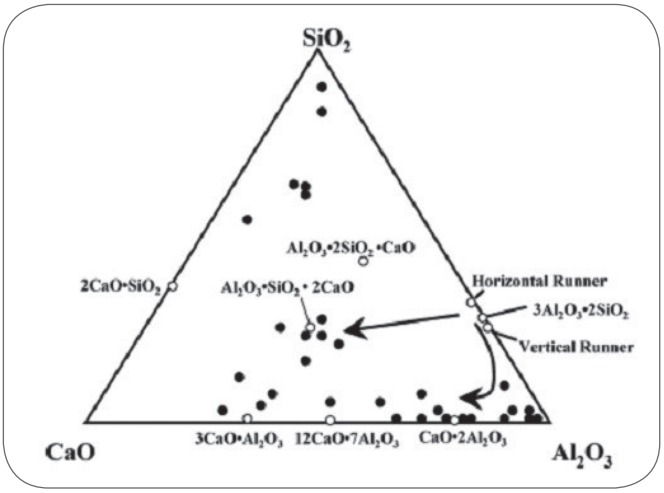

Fig. 9

Example of the pattern described on ingot A by the applied thermodynamic model following the decreasing of the oxygen potential associated with the different reactions of transformation of the metallic compounds transformed by calcium. Two main patterns starting from the mullite composition can be easily pointed and the computation well correspond with experimental measurements.
Esempio dell'evoluzione desctitta per il lingotto A attraverso l'applicazione del modello termodinamico seguendo l'andamento decrescente del potenziale di ossigeno associato con le differnti reazioni di trasformazione dei composti non metallici. I due percorsi più probabili a partire dalla composizione della mullite possono facilmente essere individuati e si nota la buona corrispondenza con le misure sperimentali.

interaction layer is almost depleted from silica, with a consequent enrichment in aluminium, iron and manganese oxides, getting ahead with the compositional change of refractory already reported in Tab. 7. Moving down the probe, it can be noted the rapid increase of Ca content, which can be explained only considering the pick up of this element from the liquid steel. Calcium reacts with Al_2O_3 producing grossite ($CaO{\cdot}2Al_2O_3$) macro-inclusions (Figs. 8(c)–8(d)); while MgO, FeO and MnO separate from them, forming spinel inclusions (Mg(1_x_y) FexMny)$O{\cdot}Al_2O_3$ (Fig. 8(c)).
Although macro-inclusions with a gehlenite composition were not individuated, the enrichment in calcium and the grossite formation prove that the interaction between refractories materials and steel can bring to the growth of high Ca-rich macro-inclusions, like those found into the steel ingots.
The forecasting of the thermodynamic model seems to correspond well with the experimental observations, because the trend of the oxygen activity associated with the chemical reactions (Tab. 8) seems to describe the pattern of the ternary diagram from the mullite composition along the non metallic macro-inclusions revealed by the metallographic examinations (Fig. 9). The high tendency to the formation of the anorthite ($2SiO_2{\cdot}CaO{\cdot}Al_2O_3$), gehlenite ($SiO_2{\cdot}2CaO{\cdot}Al_2O_3$) and grossularia ($3SiO_2{\cdot}3CaO{\cdot}Al_2O_3$) are confirmed by the composition of the non metallic inclusions on the ternary system as well as the progressive transformation from the alumina corner to the compositions occupying the centre of the $CaO–Al_2O_3$ line. Moreover, it is interesting to note that the reaction (3.1) seems to be characterized by a very low oxygen activity and so by a very great driving force. It appears reliable that the damage process of the mullite can start up by the action performed by calcium and this reaction also seems to explain the large amount of inclusions developed near the Al_2O_3 corner, because this terminal compound is a product of the damaging reaction described in reaction (3.1). The reaction (3.2) can also take place but its driving force (oxygen activity) is competitive with the other computed reactions and so it is reliable that it is not the predominant one, although some rare SiO2 macro-inclusions, probably produced by refractory aggression, have been revealed by the performed analysis. Actually, the lines which can be individuated on the diagram seem to follow the decrease in the oxygen potential to arrive at the point featured by the lowest one in which the available driving force for the transformation from the mullite composition reaches a maximum. The greater amount of gehlenite than that statistically revealed near the zone of anorthite (although the highest equilibrium oxygen activity associated to the first one indicates a lower driving force) can be due to the lower content of silica because of a minor presence within the refractories. The role played by calcium on the transformation of the refractory lining of the runners comes out to be fundamental for the development of the degradation process of the refractory and the subsequent transformation of the detached constituents. We can stress the conclusion that the calcium imposed by the strongly basic slag used for the refining plays an important role in the damaging process of the refractory and in the transformation of the attacked material; the consideration of calcium action can allow to clarify the origin of an important class of macro-defects of the ingot whose source is the runner refractory itself.
In this work a complete characterization of macro-inclusions extracted from special grade steel ingots was carried out. The results of EDS micro-analysis and Bidimensional X-ray diffraction measurements permit to conclude that the macro-inclusions are composed mainly by ghelenite ($SiO_2{\cdot}2CaO{\cdot}Al_2O_3$) and grossite ($CaO \cdot 2Al_2O_3$) crystalline phases.
The XRF and EDS analyses carried out on steel samples sectioned at the end of casting from the solidified ingot runner permit to assess the following conclusions:
(1) Exchange reactions take place between $Al_2O_3–SiO_2$ base refractory and aluminium-killed molten steel, producing the depletion of silica with a consequent increase of iron, manganese and aluminium oxide into the refractory.
(2) The horizontal runner is more affected by chemical and mechanical erosion of steel respect to the horizontal one.
(3) The wear of horizontal runner can be a source of macro-inclusion in the steel, because, in correspondence of the interaction layer, it was observed the formation of large non-metallic particles, which are completely detached from the refractory lining and free to go inside the mould producing macro-defects.
(4) these non metallic particles have a composition close to the grossite phase, as a consequence of Ca enrichment of refractory diffusion layers closer to the liquid steel.
(5) Macro-inclusions with a ghelenite composition were not individuated, but the enrichment in calcium and the grossite formation prove that the interaction between refractories materials and steel can bring to the growth of high Ca-content macro-inclusions, like those found into the steel ingots.
(6) The developed thermodynamic model based on the driving force available for each of the considered reactions has shown that there is a clear pattern leading from the chemical composition of the mullite constituting the refractory to the macro-inclusions pointed out by the metallographic observations which seems to prove that is the high activity of calcium

imposed by the slag.
(7) Two main patterns seems to be followed on the ternary SiO2–CaO–Al_2O_3 diagram by the sequential transformations of the refractories: a first one leading to the chemical composition around $CaO \cdot 2Al_2O_3$ and a second one leading toward the regions characterized by the presence of gehlenite and grossularia and this pattern seems to be well underlined also by the chemical compositions of the macroinclusions experimentally observed and it is very interesting to note that the transformation occurring on the surface layer of the refractories seems to be consistent with the ones supposed for the macro-inclusions.
(8) The aggression produced by the calcium activity due to the highly basic slag needs to be accurately considered to grant the correct cleanliness of the final ingot.

ACKNOWLEDGEMENT

The authors wish to thank Prof. Laura Eleonora Depero and Prof. Elza Bontempi (Chemical Structural Laboratory of the Brescia University) for providing the X-ray measurements and for the useful technical discussion.

NOMENCLATURE

a_i : Raoultian activity of the generic element i
γ_i : Raoultian activity coefficient for the element i
γ_i^0 : Activity coefficient for the element i at infinite dilution based on mole fraction in molten iron
ε_j^i : Interaction coefficient between the elements i and j based on mole fraction in molten iron
[ ] : Square brackets indicate the chemical species dissolved in the liquid steel
( ) : Brackets indicate the chemical species present as solid within the volume of the liquid steel
G^0 : Gibbs free energy at standard state [J mol_1]
K_{X-XO} : Constant of equilibrium for the reaction of oxidation of the species X to form the oxide XO
X_i : Molar fraction of the generic element i

REFERENCES

1) D. Xie, C. Garlick and T. Tran: ISIJ Int., 45 (2005), 175.
2) J. Fruehan: Metall. Mater. Trans. B, 28B (1997), 743.
3) Y. Fukuda, Y. Ueshima and S. Mizoguchi: ISIJ Int., 32 (1992), 164.
4) Z. Nakagawa, T. Itoh and N. Enomoto: Adavances in Refractories for the Metallurgical Industries II, CIM, Montreal, Canada, (1996), 257.
5) R. C. Rossi and R. M. Fulrath: J. Am. Ceram. Soc., 46 (1963), 145.
6) F. Oeters: Metallurgy of Steelmaking, Verlag Stahleisen mbH, Düsseldorf, (1994), 85.
7) C. Mapelli: Steel Res. Int., 77 (2006), 462.
8) I. Barin and O. Knacke: Thermochemical Properties of Inorganic Substances, Springer Verlag, Berlin, (1973).
9) I. Barin, O. Knacke and O. Kubaschewski: Thermochemical Properties of Inorganic Substances, Springer Verlag, Berlin, (1977).
10) A. Dinsdale: SGTE Data for Pure Elements, NPL Report DMA(A)195, Rev. (August 1990).
11) C. Gatellier, H. Gaye, J. Lehmann and Y. Zbaczyniak: Revue de Métallurgie-CIT, (1992), 887.
12) T. Miki and M. Hino: ISIJ Int., 45 (2005), 1848.
13) C. Bodsworth and H. B. Bell: Physical Chemistry of Iron and Steel Manufacture, Longman Group Limited, London, (1972), 486.
14) Z. Hong, X. Wuand and C. Kun: Steel Res., 66 (1995), 72.
15) V. Brabie: ISIJ Int., 36 (1996), S109.
16) H. Todoroki and K. Mizuno: ISS Transactions, Iron & Steelmaker, 30 (2003), March, 60.
17) H. Lachmund, N. Bannenberg,

ABSTRACT

ANALISI CHIMICO-MORFOLOGICA DELLE INCLUSIONI PROVENIENTI DA REFRATTARIO NEI LINGOTTI DA FORGIA

Parole chiave: acciaio, refrattari, solidificazione, trasform. di fase, acciaieria, rivestimenti, difettologia, metallografia metallurgia fisica, qualita'

La presenza di inclusioni non metalliche di tipo esogeno nell'acciaio è sporadica, ma, a causa delle loro significative dimensioni, ha un effetto deleterio sulle sue proprietà, diventando la principale causa di guasto in servizio dei componenti meccanici. Queste inclusioni sono di solito intrappolate all'interno dell'acciaio nel corso del colaggio o della solidificazione e tendono a concentrarsi in quelle regioni del lingotto che solidificano più rapidamente o in zone da cui la loro fuga per decantazione è in qualche modo ostacolata; nel caso di fucinati questa regione in origine corrisponde generalmente al piede del lingotto.
La maggior parte delle inclusioni esogene si genera per intrappolamento di polveri all'interno delle correnti presenti nella lingottiera, per processi di riossidazione che si verificano quando l'acciaio fuso viene a contatto con fonti esterne di ossigeno, come ad esempio il contatto con l'atmosfera durante il colaggio, e per usura chimica e meccanica dei refrattari. In considerazione della grande quantità di fonti di inclusioni, talvolta è molto difficile per una acciaieria valutare quale sia l'esatta origine della macroinclusione, processo indispensabile al fine di migliorare la qualità del prodotto. Questa indagine è complicata anche dal fatto che la caratterizzazione chimica delle macroinclusioni non è facile, in quanto le inclusioni hanno grandi dimensioni e composizione multifase, con una analisi chimica che può quindi cambiare da punto a punto. Per questi motivi è sempre necessaria un'attenta analisi della questione.
Nel presente lavoro è stata condotta una precisa caratterizzazione delle macroinclusioni presenti nei lingotti di acciaio destinati alla forgia e riconducibili all'erosione dei materiali refrattari, attraverso l'uso di SEM-EDS e tecniche non convenzionali di microdiffrazione ai raggi X. Al fine di spiegare l'origine di queste inclusioni è stata effettuata un'analisi dei materiali refrattari in uso ed è stato implementato un modello termodinamico che tenesse conto delle interazioni acciaio-refrattario.